A low-cost preparation of waste-based PANI/NiFe$_2$O$_4$ composite for photocatalytic hydrogen evolution

Dan Chen*, Yan Yang, Xiaonan Wang, Yao Xu, Guangren Qian

*School of Environmental and Chemical Engineering, Shanghai University, No. 99 Shangda Road, Shanghai 200444, China,
Tel. +86 2166137784; emails: dchen@shu.edu.cn, chendan_shu@hotmail.com (D. Chen), 1532436131@qq.com (Y. Yang),
1920388452@qq.com (X. Wang), 453351542@qq.com (Y. Xu), grqian@shu.edu.cn (G. Qian)*

ABSTRACT

An economical photocatalyst, waste-based PANI/NiFe$_2$O$_4$ composite was successfully synthesized from aniline wastewater, electroplating wastewater and pickling waste liquor. The obtained photocatalysts were characterized by XRD, TEM, XPS, FTIR spectra and VSM techniques. The material exhibited good magnetic property with high saturation magnetization (41.09 emu g^{-1}). After 3 h visible light irradiation, the hydrogen evolution capacity of waste-based PANI, NiFe$_2$O$_4$ and PANI/NiFe$_2$O$_4$ composite were 1.28, 5.10 and 8.94 mmol g^{-1} respectively. Among these materials, waste-based PANI/NiFe$_2$O$_4$ exhibited the optimum photocatalytic activity. Besides, waste-based PANI/NiFe$_2$O$_4$ also displayed higher photocatalytic hydrogen production than pure PANI/NiFe$_2$O$_4$ that has been studied before. Waste-based NiFe$_2$O$_4$ was responsible for the enhanced photocatalytic activity. The reaction mechanism of waste-based NiFe$_2$O$_4$ was researched in two parts: the effect of Cr^{3+} and organic impurities for structure formation of waste-based NiFe$_2$O$_4$ during in-situ polymerization process. The synthesized waste-based NiFe$_2$O$_4$ exhibited larger specific surface area and smaller grain structure than pure NiFe$_2$O$_4$, which facilitated the photocatalytic activity. Preparation of photocatalyst from wastewater could not only reduce environmental pollution but also produce new material for other application. The proposed preparation method of waste-based photocatalyst composite had great potential in the field of wastewater treatment and photocatalysis.

Keywords: Low cost; Waste-based; PANI/NiFe$_2$O$_4$; Photocatalytic hydrogen evolution

1. Introduction

Photocatalytic hydrogen generation based on semiconductor has been extensively studied since 1972 [1,2]. In recent decades, many efforts have been made to exploit highly active photocatalysts such as metal oxides [3–8], metal sulfide [9,10] and carbon-nitrogen compounds [11]. Nevertheless, high cost and low efficiency of these photocatalysts limits their application. Therefore, developing catalysts with high efficiency and low cost is critical for photocatalytic hydrogen production [12–14].

It is well-known that spinel ferrites have attracted increasing attention in the field of photocatalytic hydrogen production via water splitting [15–22]. Of all the ferrites, nickel ferrite with the chemical formula NiFe$_2$O$_4$ has made considerable research due to the suitable band gap and good chemical stability [15,18,20]. However, NiFe$_2$O$_4$ exhibits low visible-light-induced photocatalytic activity owing to the fast recombination of photoelectron-hole pairs [23]. Several methods, such as structure-design, metallic and non-metallic elements loading, and fabrication of semiconductor heterojunction have been reported to improve the photocatalytic activity and stability of NiFe$_2$O$_4$ [24–26]. Thereby, NiFe$_2$O$_4$-based novel photocatalyst was designed to enhance the photocatalytic hydrogen production efficiency. Kim et al. [27] reported that magnetically separable

* Corresponding author.

core@shell structured $NiFe_2O_4@TiO_2$ photocatalyst exhibited better hydrogen production activity than either pure TiO_2 or $NiFe_2O_4$. This was due to the effective charge transfer from TiO_2 to $NiFe_2O_4$.

As a widely used conductive polymer, polyaniline (PANI) has special electrical and optical properties. The band gap of PANI is 2.8 eV [28–31]. Recently, more and more photocatalyst composite containing polyaniline has been reported for photocatalytic hydrogen production, the hybrid effect could inhibit the recombination of photogenerated electron-hole pairs, resulting in a higher photocatalytic activity [32]. Wang et al. [33] synthesized Ag/polyaniline heterostructured nanosheets loaded with g-C_3N_4 nanoparticles that significantly enhanced photocatalytic hydrogen generation. Xu et al. [34] fabricated the polyaniline sensitized grey-TiO_2 nanocomposite to improve photocatalytic activity. The composite showed excellent separation efficiency of photoinduced electron-hole pairs.

In recent years, synthesis of catalysts from industrial waste has been extensively studied. Chen et al. [35] synthesized ferrite from electroplating wastewater and pickling waste liquor by microwave hydrothermal process. Tang et al. [36] reported that nanostructured PANI was obtained by removal of aniline via photocatalytic polymerization.

Pure PANI/$NiFe_2O_4$ has been reported in our previous work [37]. However, there is a lack of information about the preparation of waste-based PANI/$NiFe_2O_4$ from industrial waste and application to photocatalytic hydrogen. In this study, waste-based PANI/$NiFe_2O_4$ composite was successfully prepared by an in situ polymerization method. The synthesized composite exhibited higher photocatalytic hydrogen evolution than pure PANI/$NiFe_2O_4$ under visible light irradiation. Besides, a possible mechanism for the photocatalytic H_2 generation about waste-based PANI/$NiFe_2O_4$ was also discussed.

2. Experimental setup

2.1. Materials

The pickling waste liquor (PWL) and electroplating wastewater (EPW) used in this study were supplied by Shanghai Xinsheng Electroplating Co., Ltd. The aniline wastewater was provided by Shanghai Chemical Industry Park. Other reagents were commercially available and were used without further purification. The concentration of aniline was 30,869.48 mg L^{-1}. The content of major heavy metal elements in the wastewater was determined by inductively coupled plasma-atomic emission spectrometry (ICP-AES, Prodigy type, American Leeman Instrument Company, America). The operation was as follows: 5 ml pickling waste liquor and 5 ml electroplating wastewater were transferred to a 500 mL volumetric flask and diluted with 5% HNO_3. Then, the solution was filtered with 0.45 μm filter. Finally, the samples were detected by (ICP-AES). The result was shown in Table 1.

2.2. Preparation of materials

Waste-based $NiFe_2O_4$ was prepared by microwave hydrothermal method. In a typical procedure, pickling waste liquor and electroplating wastewater were mixed in

Table 1
Heavy metal content of pickling waste liquor and electroplating wastewater

Sample	Concentration (mg L^{-1})		
	Total Fe	Ni^{2+}	Cr^{3+}
PWL	40,950.40	UD^a	3,052.03
EPW	UD	897.53	UD

[a]UD related to undetected.

the volume ratio of 1:24 the molar ratio of Ni^{2+} to Fe^{3+} was adjusted to 1:2. The pH was adjusted to 13 with NaOH solution. The mixture was transferred into a Teflon reactor and autoclaved at 180°C for 1 h. The resulting product was collected by filtration, washed with deionized water, dried at 60°C under vacuum for 24 h.

Waste-based PANI/$NiFe_2O_4$ composite was synthesized by in situ polymerization method. 1.9 g waste-based $NiFe_2O_4$ and aniline wastewater (3.3 ml) were added into 50 ml of HCl solution (0.1 M), it was equivalent to 5 wt% of PANI on the composite, which was proved as an optimum value in previous work [37]. Then the slurry was stirred vigorously for 30 min. 0.25 g ammonium peroxydisulfate (APS) was dissolved in 5 ml of HCl solution (0.1 M), and the APS solution was added dropwise into the mixture with stirring in ice water bath condition. Then, the mixture was stirred for 24 h. Finally, the precipitation was filtered, washed repeatedly with deionized water, dried at 60°C under vacuum for 24 h.

Waste-based PANI was synthesized in the same preparation process without adding waste-based $NiFe_2O_4$.

For comparison, pure $NiFe_2O_4$ was synthesized by us previously [37]. Cr^{3+}-doped $NiFe_2O_4$ was also prepared by the same process using $Fe(NO_3)_3$· $9H_2O$ (0.0197 mol), $Ni(NO_3)_2$· $6H_2O$ (0.01 mol) and $Cr(NO_3)_3$· $9H_2O$ (0.0016 mol) as precursors, the concentration of the metals was referenced to Table 1.

2.3. Characterization

The materials were characterized by X-ray diffraction (XRD, Model XD-3A, Shinaduzu Co., Japan, Cu-Ka radiation, $\lambda = 0.154$ nm, 34 kv, 20 mA) with the 2θ range from 5° to 80° at a scan rate of 8° min^{-1}. Fourier-transform infrared (FT-IR) spectrum was obtained using a Perkin-Elmer System 2000 infrared spectrometer. Magnetic properties of the composite were investigated with a vibrating sample magnetometer (VSM, 7407 type, LakeShore Company, America). Heavy metal elements were detected by ICP-AES. The morphology feature was obtained by transmission electron microscopy (TEM, JEM-2100, 200KV). X-ray photoelectron spectroscopy (XPS, PHI 5000C ESCA System) measurements were carried out with a non-monochromatic Al Kα source.

2.4. Photocatalytic activity test

The photocatalytic hydrogen production was carried out in a gas-closed system under visible light irradiation. In a typical experiment, 20 mg of catalyst and 20 mg of water soluble Eosin Y were dispersed in a 20 mL solution containing 5 vol% of triethanolamine. Then, the system was thoroughly

vacuumed with nitrogen. A 300 W xenon lamp equipped with a special filter to remove UV irradiation ($\lambda > 420$ nm) was used as a visible light source. The produced gas was measured by a gas chromatograph (SP-7800, China, molecular sieve 5Å, TCD detector, and nitrogen as carrier gas).

3. Results and discussion

3.1. Morphology

The TEM images of waste-based PANI/NiFe$_2$O$_4$ were shown in Fig. 1 to confirm the hybridization between waste-based PANI and waste-based NiFe$_2$O$_4$. The dark spots of waste-based NiFe$_2$O$_4$ were hexagonal shape. It can be seen that PANI particles were immobilized on the NiFe$_2$O$_4$ carrier. The composite exhibited good dispersion and uniformity. It implied that waste-based PANI/NiFe$_2$O$_4$ was synthesized successfully, which was further corroborated by XRD results.
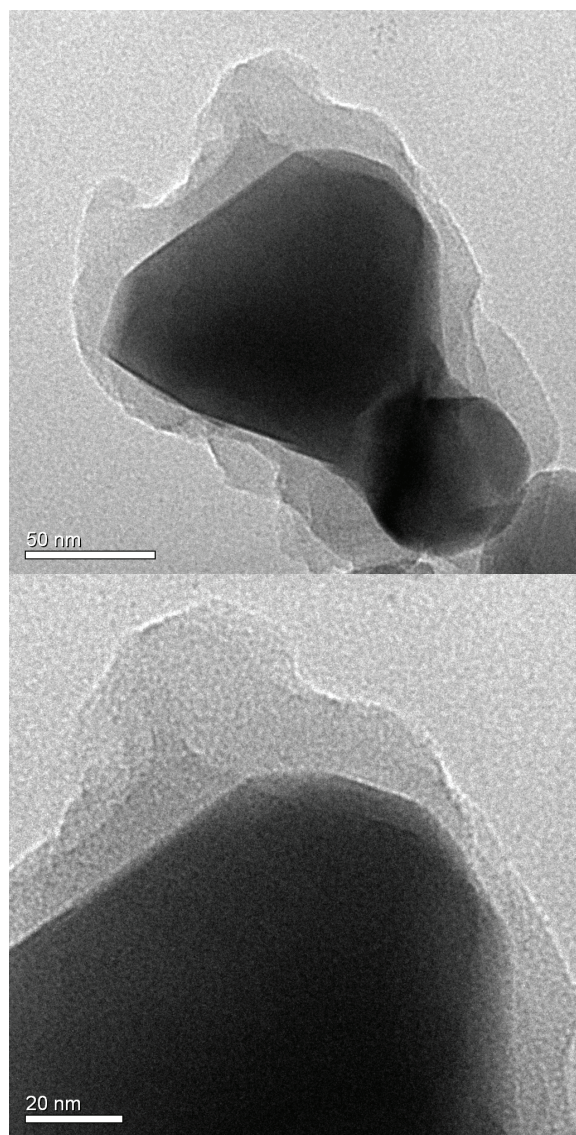
3.2. Structure characterization

Fig. 2 was the FT-IR spectrum of waste-based catalysts. For waste-based PANI/NiFe$_2$O$_4$, two bands near 1,578 and 1,492 cm^{-1}, were assigned to C=N and C=C vibrational peaks. Peaks appeared at 1,302 and 1,145 cm^{-1} were C–N and –NH$_4^+$ bending vibration. Peak at 520 cm^{-1} was Fe–O. The peaks of waste-based PANI were at around 1,556, 1,455, 1,282 and 1,230 cm^{-1}. The band at 507 cm^{-1} of waste-based NiFe$_2$O$_4$, was assigned to Fe–O. It proved that waste-based catalysts could be prepared from waste-based raw materials successfully.

The XRD patterns of waste-based 5% PANI/NiFe$_2$O$_4$ and NiFe$_2$O$_4$ were shown in Fig. 3. The diffraction peaks located at 2θ = 18.5°, 30.4°, 35.8°, 43.4°, 53.9°, 57.4° and 63.0°, were corresponding to the (111), (220), (311), (400), (422), (511) and (440) crystal planes of nickel ferrite lattice.

However, there were no characteristic peaks of polyaniline in the XRD pattern of the waste-based 5% PANI/NiFe$_2$O$_4$, which was due to the low content of polyaniline in the material.
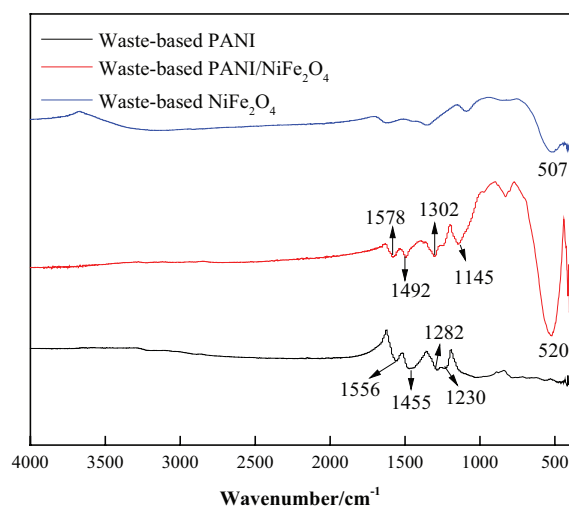

Fig. 1. TEM images of waste-based 5% PANI/NiFe$_2$O$_4$.
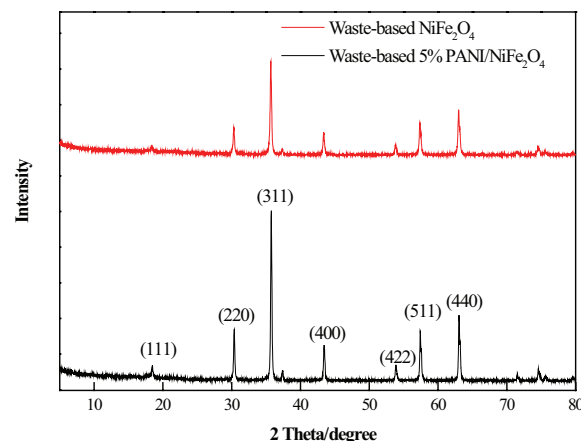

Fig. 2. FT-IR of waste-based catalysts.

Fig. 3. XRD patterns of waste-based 5% PANI/NiFe$_2$O$_4$ and waste-based NiFe$_2$O$_4$.

XPS analysis was recorded to further investigate the electronic states of samples. Fig. 4(b) exhibited the N 1s spectra of waste-based PANI/NiFe$_2$O$_4$ which demonstrated the presence of –NH$^+$/=N$^+$– (400.47 eV), –NH (399.44 eV), and =N– (398.47 eV) [38]. As shown in Figs. 4(c) and (d), the binding energies at 872.24 and 854.67 eV were attributed to Ni 2p$_{1/2}$ and Ni 2p$_{3/2}$ [39]. the peaks at 723.61 and 710.99 eV were ascribed to Fe 2p$_{1/2}$ and Fe 2p$_{3/2}$ [40], confirming that Ni and Fe in the composite were in the divalent and trivalent state, respectively.

3.3. Magnetic recovery of waste-based PANI/NiFe$_2$O$_4$

Fig. 5 was the VSM plot of waste-based 5% PANI/NiFe$_2$O$_4$. The waste-based 5% PANI/NiFe$_2$O$_4$ exhibited good magnetic recovery characteristics, and the saturation magnetization (Ms) was 41.09 emu g^{-1}. So the material could be recycled under the magnetic field condition.

3.4. Photocatalytic activity

The photocatalytic activities of various samples are shown in Fig. 6. After 3 h visible light irradiation, the photocatalytic hydrogen evolution of waste-based PANI, NiFe$_2$O$_4$ and PANI/NiFe$_2$O$_4$ were 1.28, 5.10 and 8.94 mmol g^{-1} respectively. Waste-based PANI/NiFe$_2$O$_4$ composites had higher hydrogen evolution than single waste-based PANI or NiFe$_2$O$_4$. Compared with the photocatalytic activities of pure catalysts [37], hydrogen evolution of waste-based PANI/NiFe$_2$O$_4$ and NiFe$_2$O$_4$ were obviously higher than pure PANI/NiFe$_2$O$_4$ (3 h H$_2$ evolution was 6.04 mmol g^{-1}) and NiFe$_2$O$_4$ (3 h H$_2$ evolution was 3.43 mmol g^{-1}). However, the 3 h

photocatalytic hydrogen production of waste-based PANI was slightly lower than the pure PANI (3 h H$_2$ evolution was 1.49 mmol g^{-1}). This result indicated that waste-based PANI/NiFe$_2$O$_4$ was more efficient than pure PANI/NiFe$_2$O$_4$. Furthermore, waste-based NiFe$_2$O$_4$ played an important role in the enhanced photocatalytic activity, which significantly boosted the photocatalytic H$_2$ generation. The apparent quantum efficiency (QE) of waste-based PANI/NiFe$_2$O$_4$ was calculated by Eq. (1) [41]:

$$QE\ (\%) = [\text{number of reacted electrons}/\text{number of incident photons}] \times 100 \qquad (1)$$
$$= [2 \times \text{number of generated H}_2 \text{ molecules}/\text{number of incident photons}] \times 100$$
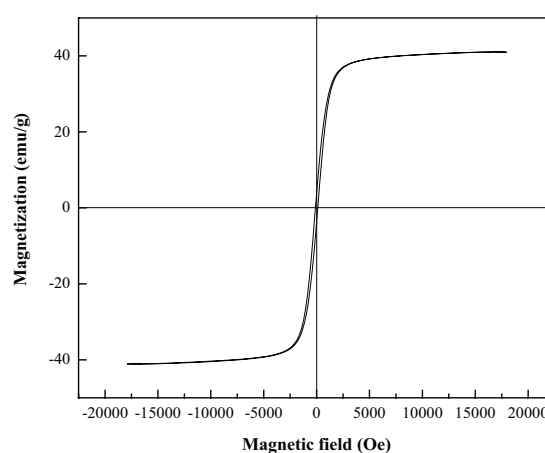
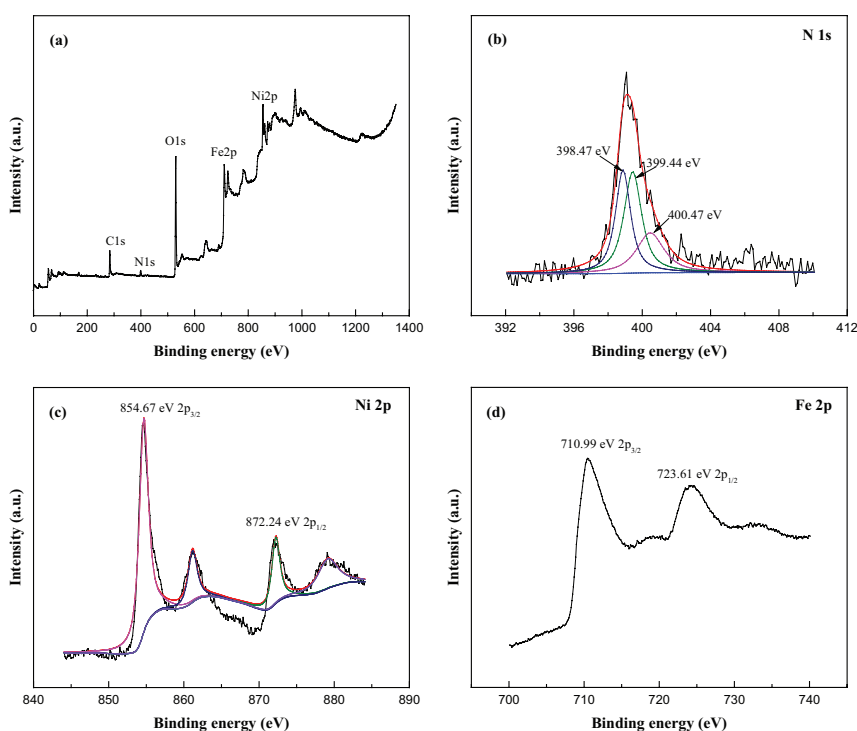Fig. 5. Hysteresis loop plot of waste-based 5% PANI/NiFe$_2$O$_4$.

Fig. 4. XPS spectra of (a) waste-based NiFe$_2$O$_4$; (b) N 1s; (c) Ni 2p and (d) Fe 2p.

The QE was measured under the similar photocatalytic activity experimental conditions at $\lambda = 420$ nm, and the calculated QE was estimated to be 0.17%.

3.5. Photocatalytic mechanism

In our previous work, the enhanced photocatalytic activity of pure $PANI/NiFe_2O_4$ was proved to the synergistic effect of PANI and $NiFe_2O_4$, which promoted the separation of photogenerated electrons and holes [37].

In this study, based on earlier photocatalytic hydrogen production results, it was proved that waste-based $PANI/NiFe_2O_4$ exhibited a better photocatalytic activity compared with pure $PANI/NiFe_2O_4$. Waste-based $NiFe_2O_4$ was responsible for the enhanced photocatalytic activity. The influence of waste-based $NiFe_2O_4$ for promoting photocatalytic activity was analyzed in two parts: the effect of Cr^{3+} and organic impurities for structure formation of waste-based $NiFe_2O_4$ during in-situ polymerization process.

3.5.1. The effect of Cr^{3+}

Recently, it has been found that the photocatalytic performance of photocatalyst could be influenced by metal doping [42]. Wen et al. [43] found that the photocatalytic hydrogen production performance of $g\text{-}C_3N_4/NiS$ was improved by doping with Ni^{2+}. Lin et al. [44] modified TiO_2 with Fe^{3+} to improve its electron transfer ability.

The main metal ions present in waste-based nickel ferrite were Ni^{2+}, Fe^{3+} and Cr^{3+}. For comparison, pure reagent Cr^{3+}-doped $NiFe_2O_4$ was synthesized using the same method. Fig. 7 shows the photocatalytic H_2 evolution of waste-based $NiFe_2O_4$ and Cr^{3+}-doped $NiFe_2O_4$. As can be seen in Fig. 7, The H_2 evolution capacity of waste-based $NiFe_2O_4$ and Cr^{3+}-doped $NiFe_2O_4$ was 5.10 and 1.87 mmol g^{-1} after 3 h visible light irradiation. By doping Cr^{3+}, the amount of H_2 evolution was decreased. Compared with pure $NiFe_2O_4$ [37], the photocatalytic H_2 evolution of Cr^{3+}-doped $NiFe_2O_4$ was lower than pure $NiFe_2O_4$. The result proved that H_2 evolution of waste-based $NiFe_2O_4$ was better than pure reagent Cr^{3+}-doped $NiFe_2O_4$, which was not due to the doping of Cr^{3+}.

3.5.2. Effect of organic complexation

Li et al. [45] and An et al. [46] reported that the presence of some organic matter can improve the photocatalytic performance by optimizing the structure of the metal oxide catalyst.

The FT-IR spectra characterization was carried out to explore the specific effect of organic impurities during in-situ polymerization process. As can be seen in Fig. 8, there were no peaks in Ni-containing electroplating wastewater. For Fe-containing pickling waste liquor, the peak observed at 3,567 cm^{-1} was attributed to –4OH. The bands at 1,747 and 1,044 cm^{-1} were C=O and C–O stretching vibration, and the bands around 1,604 and 584 cm^{-1} were assigned to the vibration of carboxyl group and Fe–O. For waste-based $NiFe_2O_4$, the bands at 1,620 and 1,352 cm^{-1} were the stretching vibration of carboxyl group and –OH. The peaks at 1,088 and 507 cm^{-1} were the C–O stretching vibration and Fe–O. It represented that complexation reaction between metals and organic impurities was happened during in-situ polymerization process.
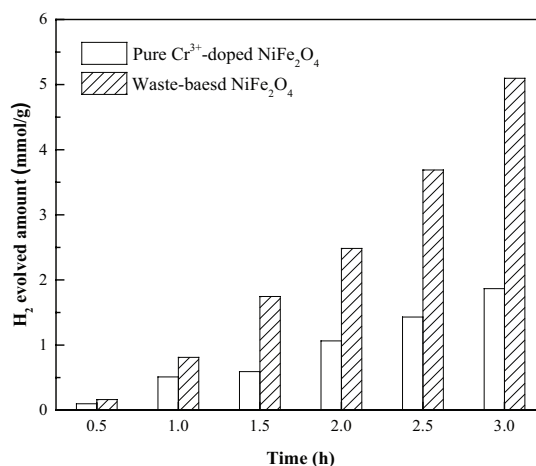
Fig. 7. Photocatalytic hydrogen production of waste-based $NiFe_2O_4$ and pure Cr^{3+}-doped $NiFe_2O_4$.

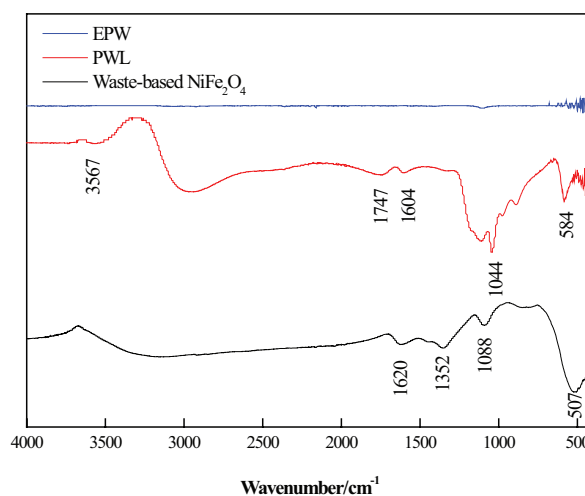Fig. 6. Photocatalytic hydrogen production of waste-based materials.

Fig. 8. FT-IR spectra of electroplating wastewater, pickling waste liquor and waste-based $NiFe_2O_4$.

Table 2
Textural properties of waste-based $NiFe_2O_4$ and pure $NiFe_2O_4$

Sample	Specific surface area ($m^2 \, g^{-1}$)	Pore size (nm)	Pore volume ($cm^3 \, g^{-1}$)
Waste-based $NiFe_2O_4$	5.684	1.824	0.074
Pure $NiFe_2O_4$	3.910	2.332	0.086

The textural properties of the catalysts are presented in Table 2. The specific surface area of waste-based $NiFe_2O_4$ was higher than that of pure $NiFe_2O_4$. Waste-based $NiFe_2O_4$ exhibited better dispersion, larger specific surface area and smaller grain structure compared with pure $NiFe_2O_4$. Therefore, organic impurities could increase the surface area and make the grain finer during in-situ polymerization process, which promote photocatalytic H_2 evolution.

In general, a possible mechanism for the photocatalytic H_2 generation about waste-based PANI/$NiFe_2O_4$ was proposed in two aspects: (1) the heterojunction of $NiFe_2O_4$ and PANI improved the separation efficiency of photogenerated e^- and h^+, which was proved by our previous work; (2) the effect of waste-based $NiFe_2O_4$, its excellent structure promoted the photocatalytic property of waste-based PANI/$NiFe_2O_4$.

4. Conclusion

In summary, a green and low-cost synthesis technology was used for the preparation of waste-based PANI/$NiFe_2O_4$ composite from pickling waste liquor, electroplating wastewater and aniline wastewater. The photocatalytic hydrogen production of waste-based PANI/$NiFe_2O_4$ was higher than pure PANI/$NiFe_2O_4$ after 3 h visible light irradiation. The H_2 evolution capacity of waste-based PANI/$NiFe_2O_4$ was 8.94 mmol g^{-1} within 3 h. It revealed that this great enhancement in photocatalytic hydrogen production was attributed to the waste-based $NiFe_2O_4$. Combined with our previous work, the significant enhanced photocatalytic activity of waste-based PANI/$NiFe_2O_4$ was ascribed to the synergistic effect of PANI and $NiFe_2O_4$. Besides, owing to the better dispersibility, larger specific surface area and smaller grain structure of waste-based $NiFe_2O_4$, which exhibited a high photocatalytic performance. So, waste-based $NiFe_2O_4$ was more efficient than pure $NiFe_2O_4$ in photocatalytic hydrogen production. Furthermore, this work provided a new idea for developing waste-based photocatalysts.

Acknowledgments

Reference

[1] M. Ni, M.K.H. Leung, D.Y.C. Leung, K. Sumathy, A review and recent developments in photocatalytic water-splitting using TiO_2 for hydrogen production, Renewable Sustainable Energy Rev., 11 (2007) 401–425.

[2] Y.H. Jiang, F. Li, Y. Liu, Y.Z. Hong, P.P. Liu, L. Ni, Construction of TiO_2 hollow nanosphere/g-C_3N_4 composites with superior visible-light photocatalytic activity and mechanism insight, J. Ind. Eng. Chem., 41 (2016) 130–140.

[3] M.G. Wang, J. Han, Y.M. Hu, R. Guo, Y.D. Yin, Carbon-incorporated NiO/TiO_2 mesoporous shells with p-n seterojunctions for sficient sisible sight shotocatalysis, ACS Appl. Mater. Inter., 8 (2016) 29511–29521.

[4] H.J. Zhang, G.H. Chen, D.W. Bahnemann, Photoelectrocatalytic materials for environmental applications, J. Mater. Chem., 19 (2009) 5089–5121.

[5] T. Song, P.Y. Zhang, J. Zeng, T.T. Wang, A. Ali, H.P. Zeng, Boosting the photocatalytic H_2 evolution activity of Fe_2O_3 polymorphs (α-, γ- and β-Fe_2O_3) by fullerene [C_{60}]-modification and dye-sensitization under visible light irradiation, RSC Adv., 7 (2017) 29184–29192.

[6] J.P. Huo, L.T. Fang, Y.L. Lei, G.C. Zeng, H.P. Zeng, Facile preparation of yttrium and aluminum co-doped ZnO via a sol–gel route for photocatalytic hydrogen production, J. Mater. Chem. A., 2 (2014) 11040–11044.

[7] T. Song, J.P. Huo, T. Liao, J. Zeng, J.Y. Qin, H.P. Zeng, Fullerene [C_{60}] modified Cr_2–xFe_xO_3 nanocomposites for enhanced photocatalytic activity under visible light irradiation, Chem. Eng. J., 287 (2016) 359–366.

[8] A. Wang, H.W. Yang, T. Song, Q. Sun, H. Liu, T.T. Wang, H.P. Zeng, Plasmon mediated Fe-O in an octahedral site of cuprospinel by Cu NPs for photocatalytic hydrogen evolution, Nanoscale, 9 (2017) 15760–15765.

[9] W.H. Feng, Z.B. Fang, B. Wang, L.L. Zhang, Y. Zhang, Y. Yang, M. Huang, S.X. Weng, P. Liu, Grain boundary engineering in organic–inorganic hybrid semiconductor ZnS(en)$_{0.5}$ for visible-light photocatalytic hydrogen production, J. Mater. Chem. A., 5 (2017) 1387–1393.

[10] Y.J. Hao, S.-Z. Kang, X. Liu, X.Q. Li, L.X. Qin, J. Mu, An efficient noble-metal-free photocatalyst for visible-light-driven H_2 Evolution: Cu/Ni-codoped $Cd_{0.5}Zn_{0.5}S$ nanoplates, ACS Sustain. Chem. Eng., 5 (2016) 1165–1172.

[11] J. Liu, Y. Liu, N.Y. Liu, Y.Z. Han, X. Zhang, H. Huang, Y. Lifshitz, S.-T.Lee, J. Zhong, Z.H. Kang, Metal-free efficient photocatalyst for stable visible water splitting via a two-electron pathway, Science, 347 (2015) 970–974.

[12] S.H. Shen, J.W. Shi, P.H. Guo, L.J. Guo, Visible-light-driven photocatalytic water splitting on nanostructured semiconducting materials, Int. J. Nanotechnol., 8 (2011) 523–591.

[13] S.H. Shen, J. Chen, X.X. Wang, L. Zhao, L.J. Guo, Microwave-assisted hydrothermal synthesis of transition-metal doped $ZnIn_2S_4$ and its photocatalytic activity for hydrogen evolution under visible light, J. Power. Sources., 196 (2011) 10112–10119.

[14] K. Meada, K. Domen, New non-oxide photocatalysts designed for overall water splitting under visible light, J. Phys. Chem., 111 (2007) 7851–7861.

[15] R. Dillert, D.H. Taffa, M. Wark, T. Bredow, D.W. Bahnemann, Research update: photoelectrochemical water splitting and photocatalytic hydrogen production using ferrites (MFe_2O_4) under visible light irradiation, APL Mater., 3 (2015) 104001.

[16] P.P. Jing, J.L. Du, J.B. Wang, W. Lan, L.N. Pan, J.N. Li, J.W. Wei, D.R. Cao, X.L. Zhang, C.B. Zhao, Q.F. Liu, Hierarchical $SrTiO_3$/$NiFe_2O_4$ composite nanostructures with excellent light response and magnetic performance synthesized toward enhanced photocatalytic activity, Nanoscale, 7 (2015) 14738–14746.

[17] A. Boudjemaa, I. Popescu, T. Juzsakova, M. Kebir, N. Helaili, K. Bachari, I.-C. Marcu, M-substituted (M = Co, Ni and Cu) zinc ferrite photo-catalysts for hydrogen production by water photo-reduction, Int. J. Hydrogen Energy, 41 (2016) 11108–11118.

[18] D. Chen, F. Zhang, Q. Li, W.D. Wang, G.R. Qian, Y.G. Jin, Z.P. Xu, A promising synergistic effect of nickel ferrite loaded on the layered double hydroxide-derived carrier for enhanced photocatalytic hydrogen evolution, Int. J. Hydrogen Energy., 42 (2017) 867–875.

[19] H.J. Lv, L. Ma, P. Zeng, D.N. Ke, T.Y. Peng, Synthesis of floriated $ZnFe_2O_4$ with porous nanorod structures and its photocatalytic hydrogen production under visible light, J. Mater. Chem., 20 (2010) 3665–3672.

[20] H.M. Gobara, I.M. Nassar, A.M.A. El Naggar, G. Eshaq, Nanocrystalline spinel ferrite for an enriched production of hydrogen through a solar energy stimulated water splitting process, Energy, 118 (2017) 1234–1242.

[21] M. Dhiman, A. Goyal, V. Kumar, S. Singhal, Designing different morphologies of $NiFe_2O_4$ for tuning of structural, optical and magnetic properties for catalytic advancements, New J. Chem., 40 (2016) 10418–10431.

[22] J. Chen, D.M. Zhao, Z.D. Diao, M. Wang, S.H. Shen, Ferrites boosting photocatalytic hydrogen evolution over graphitic carbon nitride: a case study of $(Co, Ni)Fe_2O_4$ modification, Sci. Bull., 61 (2016) 292–301.

[23] J. Zeng, T. Song, M.X. Lv, T.T. Wang, J.Y. Qin, H.P. Zeng, Plasmonic photocatalyst $Au/g-C_3N_4/NiFe_2O_4$ nanocomposites for enhanced visible-light-driven photocatalytic hydrogen evolution, RSC Adv., 6 (2016) 54964–54975.

[24] A.L. Tiano, G.C. Papaefthymiou, C.S. Lewis, J. Han, C. Zhang, Q. Li, C.Y. Shi, A.M.M. Abeykoon, S.J.L. Billinge, E. Stach, J. Thomas, K. Guerrero, P. Munayco, J. Munayco, R.B. Scorzelli, P. Burnham, A.J. Viescas, S.S. Wong, Correlating size and composition-dependent effects with magnetic, mössbauer, and pair distribution function measurements in a family of catalytically active ferrite nanoparticles, Chem. Mater., 27 (2015) 3572–3592.

[25] D.C. Hong, Y. Yamada, M. Sheehan, S. Shikano, C.-H. Kuo, M. Tian, C.-K. Tsung, S. Fukuzumi, Mesoporous nickel ferrites with spinel structure prepared by an aerosol spray pyrolysis method for photocatalytic hydrogen evolution, ACS Sustainable Chem. Eng., 2 (2014) 2588–2594.

[26] S.Gogoi, N. Karak, Biobased waterborne hyperbranched polyurethane/$NiFe_2O_4$@rGO nanocomposite with multi-stimuli responsive shape memory attributes, RSC Adv., 6 (2016) 94815–94825.

[27] H.S. Kim, D. Kim, B.S. Kwak, G.B. Han, M.-H. Um, M. Kang, Synthesis of magnetically separable core@shell structured $NiFe_2O_4$@TiO_2 nanomaterial and its use for photocatalytic hydrogen production by methanol/water splitting, Chem. Eng. J., 243 (2014) 272–279.

[28] H.Q. Liu, F. Lian, L. Zhang, M. Liu, Photocatalysis property of titania-based thin films with covalent grafting PANi as sensitizer, Adv. Mater. Res., 549 (2012) 470–473.

[29] D. Hidalgo, S. Bocchini, M. Fontana, G. Saracco, S. Hernández, Green and low-cost synthesis of PANI–TiO_2 nanocomposite mesoporous films for photoelectrochemical water splitting, RSC Adv., 5 (2015) 49429–49438.

[30] H. Xu, J.L. Zhang, Y. Chen, H.L. Lu, J.X. Zhuang, J.L. Li, Synthesis of polyaniline-modified MnO_2 composite nanorods and their photocatalytic application, Mater. Lett., 117 (2014) 21–23.

[31] T. Wang, D. Wu, Y.L. Wang, T.B. Huang, G. Histand, T.T. Wang, H.P. Zeng, One-step solvothermal fabrication of Cu@PANI core–shell nanospheres for hydrogen evolution, Nanoscale, 10 (2018) 22055–22064.

[32] X.F. Wang, G.M. Chen, J. Zhang, Synthesis and characterization of novel Cu_2O/PANI composite photocatalysts with enhanced photocatalytic activity and stability, Catal. Commun., 31 (2013) 57–61.

[33] X.F. Wang, S.J. Feng, W. Zhao, D.L. Zhao, S.H. Chen, Ag/polyaniline heterostructured nanosheets loaded with $g-C_3N_4$ nanoparticles for highly efficient photocatalytic hydrogen generation under visible light, New J. Chem., 41 (2017) 9354–9360.

[34] S. Xu, Y.D. Han, Y. Xu, H. Meng, J.L. Xu, J.B. Wu, Y. Xu, X. Zhang, Fabrication of polyaniline sensitized grey-TiO_2 nanocomposites and enhanced photocatalytic activity, Sep. Purif. Technol., 184 (2017) 248–256.

[35] D. Chen, C.Y. Mei, L.H. Yao, H.M. Jin, G.R. Qian, Z.P. Xu, Flash fixation of heavy metals from two industrial wastes into ferrite by microwave hydrothermal co-treatment, J. Hazard Mater., 192 (2011) 1675–1682.

[36] H.Q. Tang, J. Li, Y.Q. Bie, L.H. Zhu, J. Zou, Photochemical removal of aniline in aqueous solutions: switching from photocatalytic degradation to photo-enhanced polymerization recovery, J. Hazard Mater., 175 (2010) 977–984.

[37] D. Chen, F. Zhang, W.D. Wang, Y. Yang, G.R. Qian, Synergistic effect of PANI and $NiFe_2O_4$ for photocatalytic hydrogen evolution under visible light, Int. J. Hydrogen Energy., 43 (2018) 2121–2129.

[38] T.Z. Zhou, C.P. Li, H.L. Jin, Y.Y. Lian, W.M. Han, Effective adsorption/reduction of Cr(VI) oxyanion by halloysite@ polyaniline hybrid nanotubes, ACS Appl. Mater. Inter., 9 (2017) 6030–6043.

[39] Y. Tomita, H. Nasu, Y. Izumi, J. Arai, Y. Otsuka, Y. Yamane, K. Yamada, Y. Kohno, K. Kobayashi, Synthesis and charge-discharge properties of LiF-NiO composite as a cathode material for Li-ion batteries, J. Power Sources, 329 (2016) 406–411.

[40] P.M. Rao, X.L. Zheng, Unique magnetic properties of single crystal gamma-Fe_2O_3 nanowires synthesized by flame vapor deposition, Nano Lett., 11 (2011) 2390–2395.

[41] D.P. Kumar, S. Hong, D.A. Reddy, T.K. Kim, Ultrathin MoS_2 layers anchored exfoliated reduced graphene oxide nanosheet hybrid as a highly efficient cocatalyst for CdS nanorods towards enhanced photocatalytic hydrogen production, Appl. Catal. B, 212 (2017) 7–14.

[42] I. Majeed, M.A. Nadeem, E. Hussain, G.I.N. Waterhouse, A. Badshah, A. Iqbal, M.A. Nadeem, H. Idriss, On the Synergism between Cu and Ni for photocatalytic hydrogen production and their potential as substitutes of noble metals, Chem. Cat. Chem., 8 (2016) 3146–3155.

[43] J.Q. Wen, J. Xie, H.D. Zhang, A.P. Zhang, Y.J. Liu, X.B. Chen, X. Li, Constructing multifunctional metallic Ni interface layers in the $g-C_3N_4$ nanosheets/amorphous NiS heterojunctions for efficient photocatalytic H_2 generation, ACS Appl. Mater. Inter., 9 (2017) 14031–14042.

[44] L. Lin, H.Y. Wang, W.B. Jiang, A.R. Mkaouar, P. Xu, Comparison study on photocatalytic oxidation of pharmaceuticals by TiO_2-Fe and TiO_2-reduced graphene oxide nanocomposites immobilized on optical fibers, J. Hazard Mater., 333 (2017) 162–168.

[45] F.-B. Li, J.-J. Chen, C.-S. Liu, J. Dong, T.-X. Liu, Effect of iron oxides and carboxylic acids on photochemical degradation of bisphenol A, Biol. Fertil. Soils, 42 (2006) 409–417.

[46] T.C. An, J.X. Chen, G.Y. Li, X.J. Ding, G.Y. Sheng, J.M. Fu, B.X. Mai, K.E. O'Shea, Characterization and the photocatalytic activity of TiO_2 immobilized hydrophobic montmorillonite photocatalysts, Catal. Today, 139 (2008) 69–76.